Predicting friction under vastly different lubrication scenarios

Yulong Li,[1,2,*] Peter Gumbsch,[1,3] and Christian Greiner[1,2,†]
[1]*Institute for Applied Materials (IAM), Karlsruhe Institute of Technology (KIT), Kaiserstrasse 12, 76131 Karlsruhe, Germany*
[2]*MicroTribology Center (μTC), Strasse am Forum 5, 76131 Karlsruhe, Germany*
[3]*Fraunhofer IWM, Wohlerstrasse 11, 79108 Freiburg, Germany*

(Received 8 November 2025; accepted 30 March 2026; published 22 April 2026)

Friction is ubiquitous in daily life, from nanoscale machines to large engineering components. By probing the intricate interplay between system parameters and frictional behavior, scientists seek to unveil the underlying mechanisms that enable prediction and control of friction—an essential step toward carbon neutrality. Yet, reproducing frictional behavior in experiments is notoriously difficult. Here, we experimentally show that this challenge stems from the extreme sensitivity of tribological systems to tiny variations, e.g., in surface topography, typically presumed well controlled. Even after meticulous surface preparation to semiconductor industry standards and curtailing misalignment-induced oscillations, subtle variations remain and interact. In turn, such minute initial differences lead to statistically significant variations in friction and wear, giving rise to system-level chaotic behavior. Yet, by leveraging mid-scale features of surface topography and misalignment-induced oscillations—information often filtered out or overlooked—we established a predictive framework for high-friction regions under vastly different lubrication scenarios. While no single identified descriptor robustly predicts high friction, their combined occurrence provides strong predictive ability, which is further enhanced by machine learning.

DOI: 10.1103/bx4g-8647

I. INTRODUCTION

Researchers estimate that about 23% of mankind's primary energy usage goes into overcoming friction forces and causing material wear [1]. This highlights the critical role of tribology—the study of friction, wear, and lubrication—in efforts to reduce CO_2 emissions. Since Leonardo da Vinci first articulated the "laws" of sliding friction in 1493, scientists have strived to predict friction in order to build on existing results and design tailored low-friction systems—an endeavor with the potential to save a quad of energy (10^{15} BTU) [2], equivalent to 10^{18} J. However, every scientist studying tribological systems knows how extremely hard, or truth be told, impossible, it is to precisely reproduce frictional behavior. This irresistibly calls to Eduard Lorenz's description of chaos: "When the present determines the future but the approximate present does not approximately determine the future." Such complexity of tribological experiments is especially problematic as tribology often lacks attention and remains a small field of study, while being of immense importance. Friction, a fundamental aspect of tribology, presents significant reproducibility challenges [3], making prediction even more difficult: Minor deviations in environmental conditions [4], material properties [5], or surface topography [6,7] can lead to variations of up to 20% between laboratories and up to 13% within the same laboratory, even when researchers strictly control conditions. Beyond various strategies to enhance reproducibility through improved experimental and statistical design [3,8], uncovering the root causes of irreproducibility may reveal predictors for friction behavior—an insight that lies at the core of this study's contribution.

II. METHODS

The tribological experiments were performed using a pin-on-disk configuration with pins and disks fabricated from 100Cr6 bearing steel (AISI 5210). Disks had a diameter of 70 mm and a nominal hardness of 800 HV, achieved through hardening and tempering. The disks' surface preparation involved using a cup grinding machine (G&N MPS 2 R300) equipped with a corundum grinding wheel (grit EK200), resulting in an average R_a from 0.08 to 0.12 μm (measured by HOMMEL ETAMIC T8000 R120-400). Radial height variations along the disks' sliding track were controlled to remain below 2 μm, measured using a chromatic white light profilometry (FRT MicroProf MPR 1024). Maintaining the height variation within 2 μm for the 132 mm sliding track is the minimum standard achievable in our laboratory. The pins, initially 8 mm diameter spheres and with a hardness of around 700 HV, were ground and polished to a circular flat area with a diameter of 7.33 mm, achieving R_a between 0.02 and 0.04 μm, and flatness under 0.6 μm.

All 13 experiments were conducted under consistent experimental conditions, with variations only in the interfacial media. Six lubricated experiments employed FVA 1 base oil

*Contact author: yulong.li@kit.edu
†Contact author: christian.greiner@kit.edu

Published by the American Physical Society under the terms of the Creative Commons Attribution 4.0 International license. Further distribution of this work must maintain attribution to the author(s) and the published article's title, journal citation, and DOI.

(Klueber Lubrication). Five abrasive experiments involved water-based alumina abrasive slurries with 5 μm particle sizes, resulting in high friction forces, purchased from Joke (lapping medium BIOLAM®) with a nominal concentration of 12.5 wt%. One experiment utilized Aral SuperTronic K 5W-30 engine oil (Aral). One experiment used AeroShell Grease 33 (Shell).

All experiments were conducted on a custom-modified CSEM tribometer (from CSM Instruments, now owned by Anton Paar). A normal force of 2 N was applied to the pin using dead weights with a mean sliding radius of 21 mm. The friction force was determined by measuring the deflection of the tribometer's elastic arm. Custom modifications to the CSEM tribometer included the addition of a metal block that moved coaxially with the disk and a capacitive sensor (E+H Metrology AW 210-52-1; see the Appendix in the Supplemental Material [27]) positioned on the same horizontal plane as the metal block, serving as a zero-position trigger.

Detailed methods for data processing are described in the Appendix in the Supplemental Material [27].

III. RESULTS

The inescapable interplay between frictional behavior and surface topography is present in every tribological system [9]. Surface topography, shaped by various physical effects and often exhibiting self-affine fractal properties, is highly complex and inherently irreproducible in fine detail [10,11]. This characteristic may lead tribological systems to exhibit chaotic behavior, where minute changes in initial conditions—such as the surface topography of the contacting partners—may exert unexpected and significant effects. To probe the above, we performed tribological experiments that were on purpose very fundamental and basic, while reducing potential influencing factors. We chose a classical pin-on-disk setup [in Fig. 1(a)] and one of the most common bearing steels, 100Cr6 also known as AISI 5210, for both the pin and the disk side. A normal load of 2 N was applied directly to the pin using a dead weight loading, and the friction force was determined from the deflection of the pin holder. Each individual experiment was performed using a fresh pin and disk. A flat-ended pin was deliberately selected over a spherical one to create a well-defined, constant contact area with lower nominal contact stress. This design choice minimizes the influence of an evolving pin geometry during test and allows the study to focus on how disk surface topography affects friction behavior. To ensure the broad applicability of our results, we performed tests for a wide variety of tribology conditions at room temperature: with a nonadditive base oil, a fully formulated engine oil, an aerospace grease, and an alumina slurry.

A. Surface topography's influence on friction

Given that every surface topography is unique, we aimed to minimize differences between them by keeping the disks as flat as possible, ensuring that the surface profiles' [in Figs. 1(a)–1(e) and Fig. S1 of the Supplemental Material [27]] height variation of all disks was less than 2 μm along 132 mm sliding track. The three-dimensional topography data, acquired via chromatic white light profilometry, were angularly averaged to yield a two-dimensional profile representation [Fig. 1(a)]. An example profile from a disk with a maximum height variation of 1.2 μm over the 132 mm radius is shown in Figs. 1(a) and 1(b). Surface profiles were sampled at 120 evenly spaced angular positions along the track, providing a spatial resolution of 1.1 mm. This implies that the analysis captures and focuses on mid-scale surface topography, while suppressing small-scale roughness. In highly precise semiconductor manufacturing, e.g., for the 7 nm node lithography process, a height variation of up to 5 μm is tolerated on a 300 mm wafer [12], demonstrating the precision of our disk preparation in comparison; our disks for all intents and purposes can be considered "flat" as far as tribological experiments are concerned.

When plotting the disk angle-resolved friction forces (evaluated over a sliding distance of 0–50 m) with the disk surface profile presented in Fig. 1(b), the peak in the angularly resolved friction force (30°–120°) coincides with the peak in the surface topography (10°–150°). Apart from its height, the surface texture at the peak shows no significant difference from other regions. This indicates that even tiny deviations on the surface [1 μm along a 132 mm sliding track in Fig. 1(b)] can significantly increase friction, by up to 300% in this case. In a similar vein, the high-friction section also shows more wear scratches than the low-friction section (in Fig. S2 of the Supplemental Material [27]). The correlation between surface profile height and friction emerges as a pervasive characteristic across diverse lubrication scenarios—base oil [around 90° in Fig. 1(b)], abrasive slurry [around 100° in Fig. 1(c)], engine oil [around 230° in Fig. 1(d)], and grease [around 120° in Fig. 1(e)]—despite nearly an order of magnitude difference in their absolute friction levels.

However, comparing friction across different lubrication scenarios poses challenges. As shown in Fig. 2(a), both friction force values and their trends differ significantly under abrasive wear and base oil. Nevertheless, the angular position of peak friction averaged over sliding distances of 0–50 and 50–100 m remains remarkably stable, appearing consistently near 100° under abrasive wear [Fig. 2(b)] and approximately 90° under base oil [Fig. 2(c)]. But under abrasive wear, continuous material removal leads to progressive changes in friction behavior over time, as illustrated by the 100–150 m interval in Fig. 2(b). Therefore, in this study, the angular friction values are based on the average friction within the initial 0–50 m sliding distance, in order to capture the influence of the pristine surface topography on friction.

Then, it is a challenge to identify a statistical method that enables meaningful comparison across friction data exhibiting large quantitative disparities. For example, friction value under abrasive slurry and base oil differ significantly when analyzed as a function of time [Fig. 2(a)] or position [Figs. 2(b) and 2(c)]. To address this, we standardized the friction data using the Z score. In simple terms, the Z score tells us how much a local friction value differs from the average value on the disk, relative to the overall spread of the data (details in the Appendix in the Supplemental Material [27]). Because it is dimensionless, it allows results from different experimental conditions to be compared directly. Thus, even though the absolute friction values in Figs. 2(b) and 2(c) differ by orders

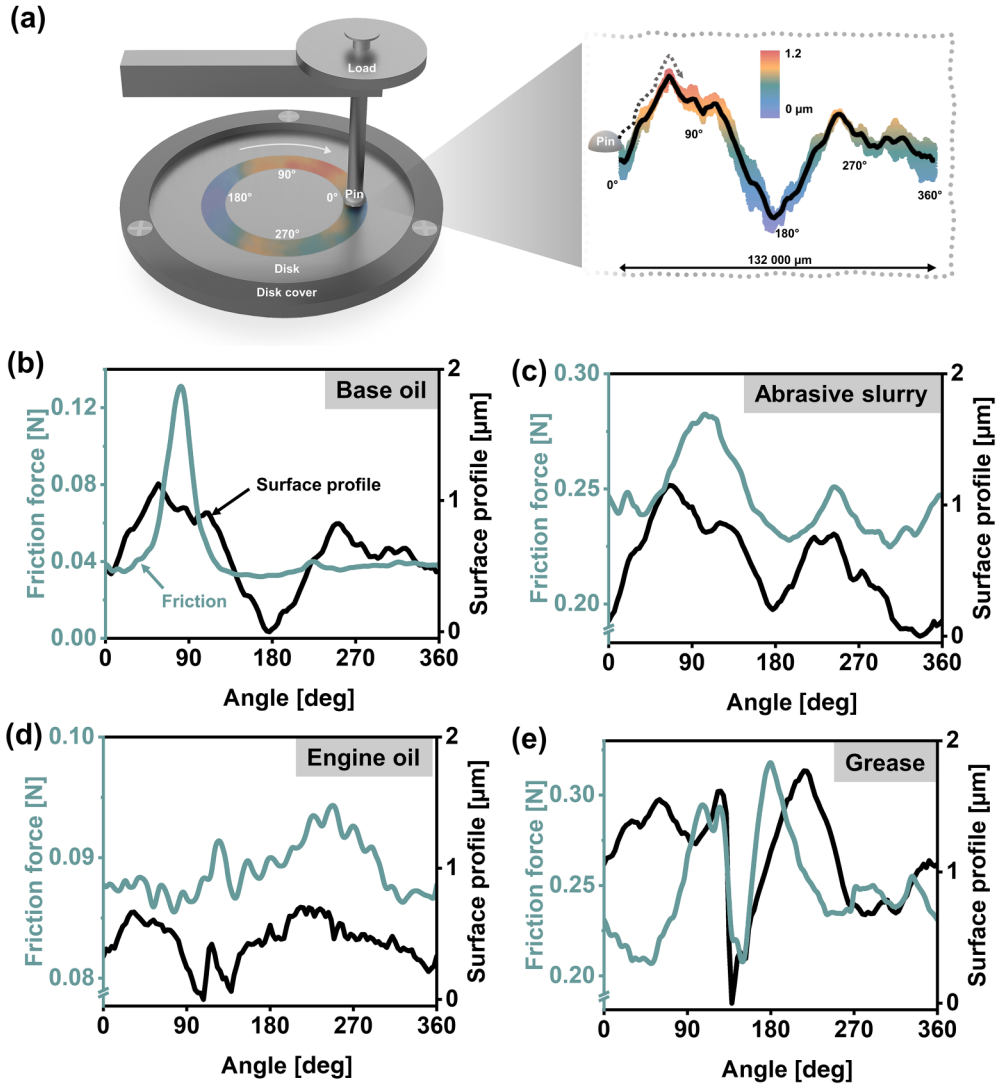

FIG. 1. Comparison of disk surface profile and friction. (a) Pin-on-disk setup. The disk rotates clockwise with the normal load applied to the fixed pin. The disk surface profile along the contact area is extracted from chromatic white light profilometry data before the tribological test. (b)–(e) Comparison of disk angle-resolved friction forces with the disk surface profile under different lubrication scenarios—base oil [panel (b)], abrasive slurry [panel (c)], engine oil [panel (d)], and grease [panel (e)]. The disk angle-resolved friction force was evaluated over a sliding distance of 0–50 m (approximately 379 disk revolutions) by segmenting the entire 132 mm sliding track (360°) into 120 equal sections.

of magnitude, the Z score in Fig. 2(d) puts them on the same scale. The 132 mm (360°) sliding track in each experiment was divided into 120 sections, and a dimensionless friction Z score was calculated for each section. The Z score corresponding to the average friction over 0–50 m, shown in Figs. 2(b) and 2(c), are summarized in Fig. 2(d).

Friction Z score and surface profile height Z score from 13 experiments were calculated (Fig. S3 of the Supplemental Material [27]), and data from all sections (1560 in total) were pooled together [Fig. 2(e)]. By focusing specifically on the 15° regions (5 out of 120 sections) of each disk's surface profile exhibiting the highest friction forces—marked in red—we observed that 74% of these sections had positive surface profile height Z score. This suggests that elevated regions in the surface profile are associated with higher friction.

This demonstrates that high peaks on the surface profile are important in the tribological contacts; at the same time, local contact conditions, such as surface curvature, might be critical as well [13]. The corresponding surface curvature for the surface profile in Fig. 1(b) is shown in Fig. S4 of the Supplemental Material [27] . Here, positive curvature corresponds to regions where the surface profile is locally concave upward (peaklike), whereas negative curvature corresponds to concave downward regions (valleylike). Similarly, we pooled the surface curvature and friction Z-score data for each section from the 13 experiments [Fig. 1(f)]. Doing so reveals that 69% of sections with friction Z score greater than 2 exhibit positive curvature, indicating a correlation between surface curvature and higher friction. This means that despite our extensive efforts to control and most importantly minimize surface topography to a standard close to that in the

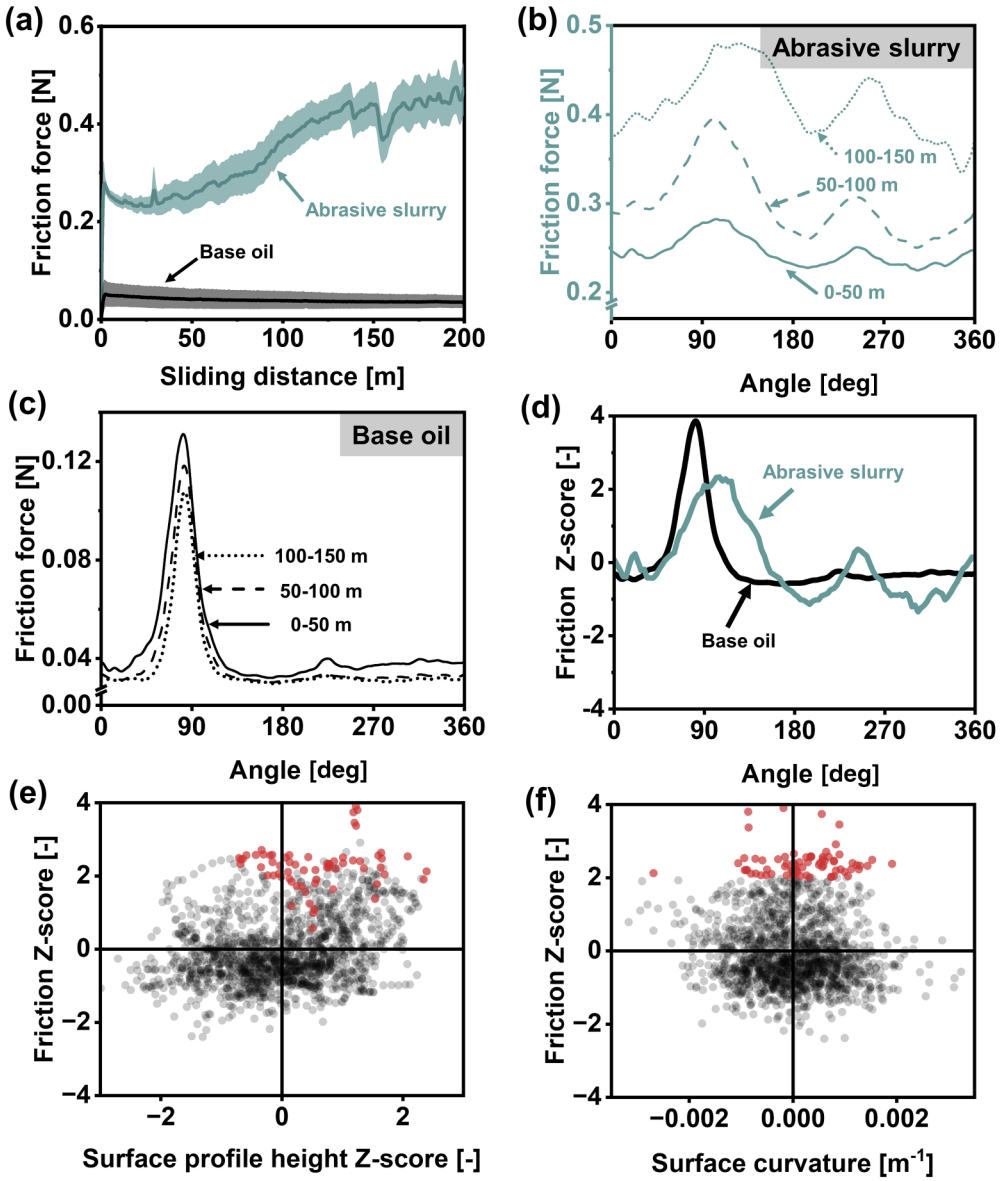

FIG. 2. Standardization of friction force and surface topography. The surface profile height Z score and surface curvature are derived from measurements of the initial surface topography before the tribological test. (a) Friction coefficient vs sliding distance. (b), (c) Angle-resolved friction forces under abrasive wear and base oil conditions at sliding distance intervals of 0–50, 50–100, and 100–150 m. Peak friction consistently appears near 100° under abrasive wear and approximately 90° under base oil. (d) Dimensionless Z scores enable direct comparison of angle-resolved friction under base oil and abrasive slurry conditions, here shown as frictional data for sliding distances of 0–50 m. (e) Friction Z score against surface profile height Z score for all 1560 sections from 13 experiments. The 15° region (5 out of 120 sections) of each disk surface profile with the highest friction is highlighted in red; 74% of these sections have a positive surface profile height Z score. (f) Friction Z score plotted against surface curvature. Sections with Z score greater than 2 are highlighted in red; 69% of these sections possess a positive curvature.

semiconductor industry, its influence on friction and wear remains significant.

B. Oscillation's influence on friction

In tribological systems, beyond surface topography, there are further parameters that cannot, realistically, be precisely controlled. For a pin-on-disk configuration, pin inclination can affect friction [14]. Disk alignment [15] is another factor that should be considered. Achieving perfect alignment and true perpendicular normal loading between pin and disk in reality is impossible. Consequently, a minuscule degree of tilt between disk and pin is inevitable, as illustrated in Fig. 3(a). This inherent misalignment in turn leads to what we have termed as oscillations. While making every effort to minimize the amplitude of these oscillations, in our experiments, the oscillation amplitude was still at least 4 μm over a 132 mm sliding track (evaluated with a capacitive sensor in Fig. S5 of the Supplemental Material [27]). The oscillation signal shown in Figs. 3(b)–3(e) represents an average over 30 disk rotations.

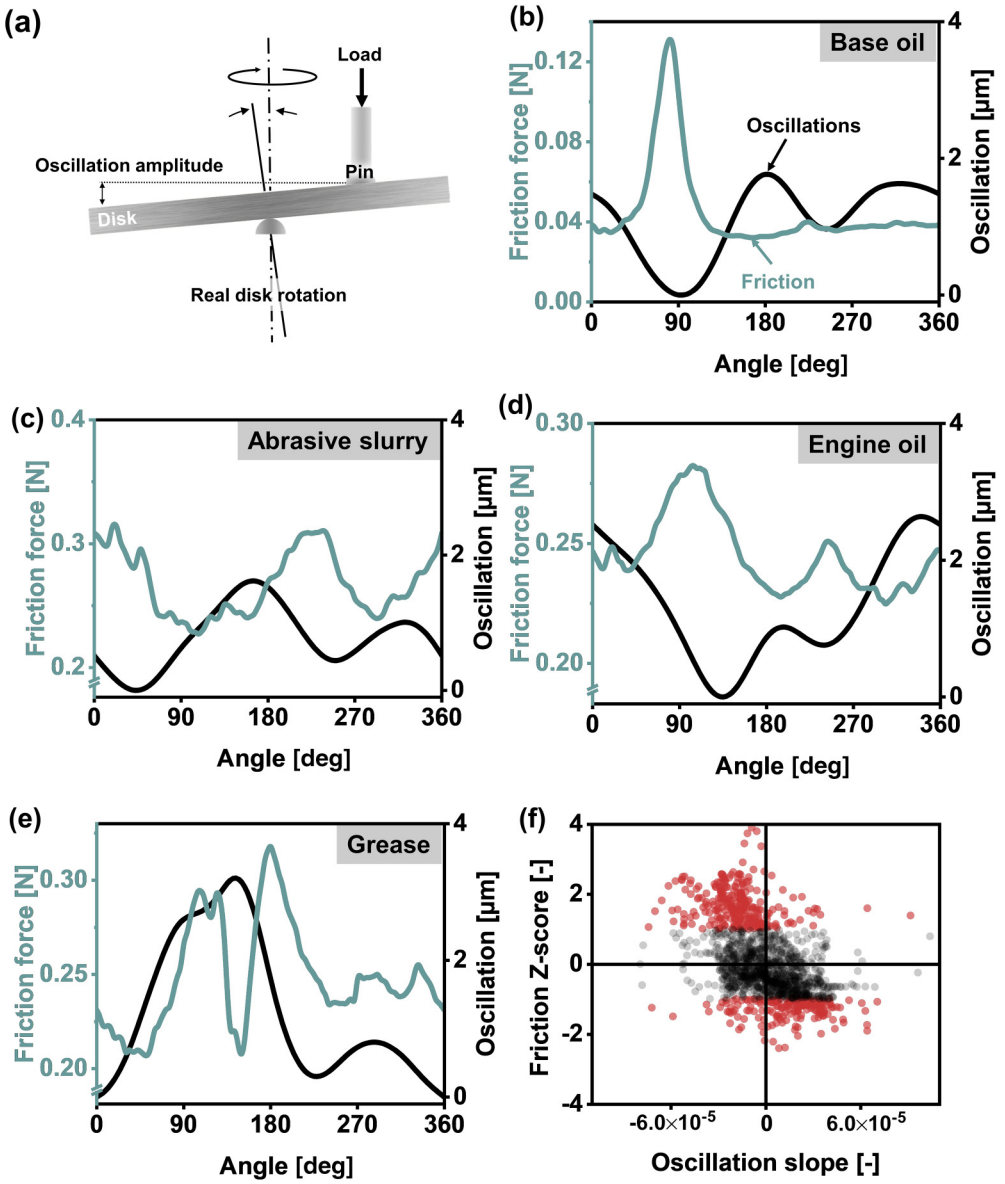

FIG. 3. Comparison of disk oscillation and friction. (a) Realistic disk rotation scenario, in which tilting during disk mounting is inevitable. This mounting-induced tilting is measured and defined as the oscillation, with the minimum oscillation value taken as the zero reference. Comparing angle-resolved friction with oscillations under different lubrication scenarios—base oil [panel (b)], abrasive slurry [panel (c)], engine oil [panel (d)], and grease [panel (e)], using data from the same experiment as in Figs. 1(b)–1(e). (f) Friction Z score against oscillation slope, using data from the same 13 experiments as in Figs. 1(c) and 1(d). Sections where the friction Z score exceeds 1 are highlighted in red, and 86% of these regions demonstrate a negative oscillation slope.

The oscillations presented in Figs. 3(b)–3(e) stem from the very same experiment as the topography and friction data shown in Figs. 1(b)–1(e). While Figs. 1(b)–1(e) capture the static surface morphology of the disks, Figs. 3(b)–3(e) reflect their dynamic changes. In comparison to the disk's topography, the correlation between the oscillation profile and the angle-resolved friction forces is not intuitively obvious. To develop such an understanding, we plot the friction Z score for each disk section from all 13 experiments against the oscillation slope [the slope of each section on the oscillation curve, illustrated in Fig. S4(b) of the Supplemental Material [27]]; the remaining nine experiments are presented in Fig. S6 of the Supplemental Material [27]; as shown in Fig. 3(f), a negative correlation between friction Z score and the oscillation slope is found. This is particularly true for regions of the disks where friction forces are deviating by more than one standard deviation from the mean value—red data points. When the Z score exceeds 1, 86% of these sections exhibit a negative oscillation slope; conversely, when the Z score is less than -1, 80% of regions exhibit a positive oscillation slope. Although the effect of oscillation-induced friction variation has been studied [16], it is remarkable that even under such minimal conditions—where we minimized contact surface oscillations to just 4 μm across a 132 mm sliding track—86% of high-friction sections

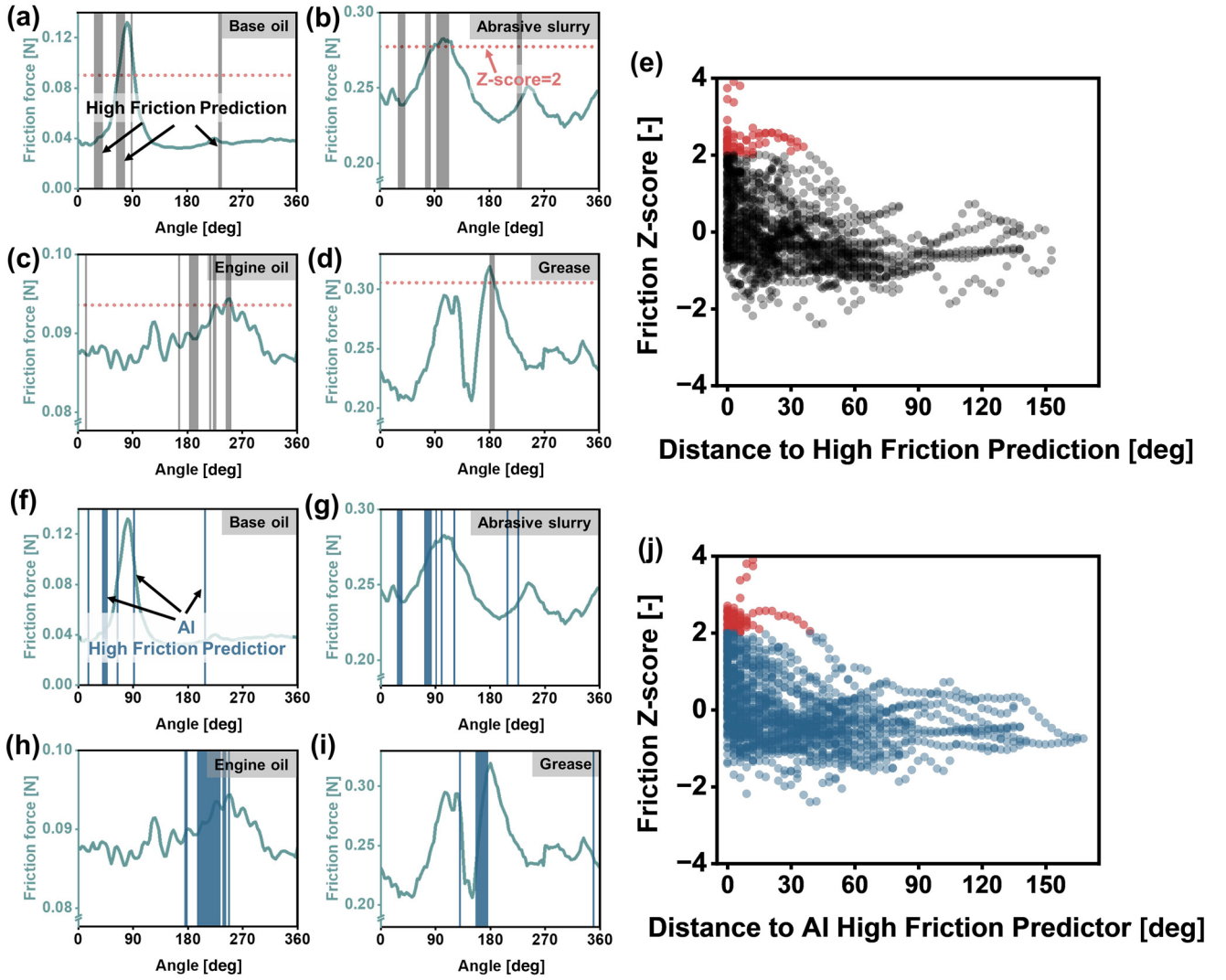

FIG. 4. High Friction Prediction [panels (a)–(e)] and AI High Friction Predictor [panels (f)–(j)]. The four experiments under different lubrication scenarios—base oil [panels (a) and (f)], abrasive slurry [panels (b) and (g)], engine oil [panels (v) and (h)], and grease [panels (d) and (i)]—correspond to the experiments shown in Figs. 1(b)–1(e) and Figs. 2(b)–2(e). (a)–(d) High friction in a simple model is predicted in sections on the sliding track that simultaneously meet three physical conditions: a negative oscillation slope, a positive surface profile height Z score, and a positive surface curvature. (f)–(i) Using a k-nearest neighbors (kNN) machine learning algorithm for classification, the regions likely to generate high friction are identified with the AI High Friction Predictor. Friction Z score for each disk section across all 13 experiments were plotted against their angular distance from the predicted high-friction region (set to zero), using both the High Friction Prediction [panel (e)] and the AI High Friction Predictor [panel (j)]. High friction sections with Z score >2 (red) consistently clustered near the predicted regions: 74% within 12° for the High Friction Prediction [panel (e)] and 86% within 12° for the AI High Friction Predictor [panel (j)].

(with the Z score exceeding 1) from 13 experiments statistically tend to occur when the disk oscillates downward.

C. High Friction Predictor

Leveraging statistical insights into how initial surface topography and oscillation influence frictional behavior before tribological contact, we sought to establish a model to identify regions on the disk where high friction is likely to occur. With the above results, High Friction Prediction is defined in regions from each disk's 120 sections that simultaneously meet three physical conditions: a negative oscillation slope, a positive surface profile height Z score, and a positive surface curvature. Even under severely different lubrication scenarios—base oil [Fig. 4(a)], abrasive slurry [Fig. 4(b)], engine oil [Fig. 4(c)], and grease [Fig. 4(d)]—the regions of highest friction consistently tend to overlap with the High Friction Prediction. A clear overlap is observed in the last three cases and close proximity in the case of the base oil. The reliability of this prediction of high friction is further demonstrated across nine repeated experiments in Fig. S7 of the Supplemental Material [27]. When plotting the friction Z score for each disk section from all 13 experiments against the angular distance of each section from the High Friction Prediction [(in Fig. 4(e)], we observe that all regions exhibiting high friction (Z score >2, red data points) are located within 36° of the High Friction Prediction, with 74% of these concentrated within 12°.

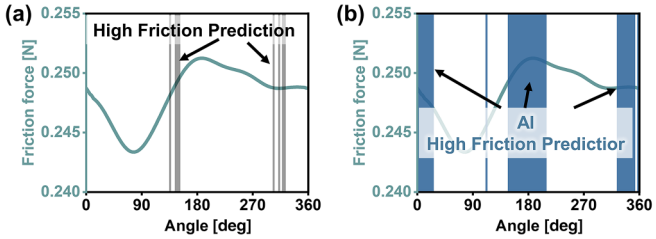

FIG. 5. Generalization of friction predictions from flat-on-flat to ball-on-flat contact. To validate the generality of the physical effects identified in this work, the models developed in Fig. 4 were applied to a ball-on-flat contact condition, using the same base oil as the lubricant. The predictions from the physics-based models in Figs. 4(a)–4(e) are shown in panel (a), while the predictions from the AI-based model in Figs. 4(f)–4(j) are shown in panel (b). Despite the complete change in contact geometry, both models remain applicable, demonstrating the generalizability of the proposed predictive framework.

With the aid of artificial intelligence (AI), we further enhanced the predictive capability. We employed the (kNN) algorithm for classification, using oscillation slope, profile height Z score, and surface curvature as input features, while the friction Z score was designated as the target to identify regions where high friction might occur (friction Z score $>$ 1). During the machine learning process, all 13 experimental datasets were utilized with 13-fold cross-validation. In this approach, each experiment was sequentially treated as the test set to generate the *AI High Friction Predictor*, while the remaining 12 experiments served as the training set. In a single experiment, comparing the AI predictor [Figs. 4(f)–4(i)] and the simple model [Figs. 4(a)–4(d)]—or the corresponding experiments shown in Figs. S7 and S8 of the Supplemental Material [27]—reveals similarities; but it is challenging to evaluate which performs better. Therefore, in Fig. 4(j), the friction Z score for each disk section across all 13 experiments was plotted against the angular distance of each section from the *AI High Friction Predictor*, we observed that 86% of the high friction regions (Z score $>$2, red data points) were concentrated within 12°. This represents a 12% improvement over our classical model [the High Friction Prediction in Fig. 4(e)]. Across all 13 experiments, the *AI High Friction Predictor* accurately located the highest friction points in eleven experiments.

To further validate the reliability of the two models presented in Fig. 4 and examine generality of the underlying physical mechanisms, a verification experiment was conducted in Fig. 5. In this experiment, the previously used flat pin was replaced with a conventional spherical pin (10 mm in diameter) made of the same material, thereby changing the contact configuration from flat-on-flat to ball-on-flat. The lubricant used was the same base oil as in Fig. 2(b). Using the models in Fig. 4, along with surface topography and oscillation data (shown in Fig. S9 of the Supplemental Material [27]), predictions were generated before the tribological experiments. The prediction and experimental results are presented in Fig. 5.

The High Friction Prediction derived from the physical-based model lies within the high-friction regime in Fig. 5(a), with a deviation of approximately 30° from the experimentally observed highest-friction position. However, in Fig. 5(b), the *AI High Friction Predictor* shows complete coincidence with the region of highest friction.

IV. DISCUSSION

Measuring surface topography, particularly roughness, and considering its effect on friction and wear is a long-standing focus in tribology. Therefore, numerous successful models have been developed and adopted to predict tribological behavior [17,18]. Yet, even when all (seemingly) relevant parameters are specified, pinpointing where the highest friction will occur on stringently controlled surfaces remains very challenging. In turn, this is exactly what is needed to know where a tribological surface should be prepared differently, or where the system most likely will fail due to excessive wear. Our experimental findings highlight the complexity behind this goal and why it has not yet been achieved. We have identified two surface features—the profile height and surface curvature—that are highly predictive of high friction events. However, the relationship between these parameters and the frictional forces remains somewhat chaotic, as neither factor alone robustly predicts high-friction [see Figs. 1(b)–1(e)].

This complexity arises largely because misalignment-induced oscillations, even when minimized, continuously influence friction behavior. The reproducibility challenge in friction can arise from surface topography and oscillations and their complex interactions that may ultimately give rise to system-level chaotic behavior. This chaotic nature is evidenced by positive Lyapunov exponents [19] calculated for the friction data shown in Figs. 1(b)–1(e). The Lyapunov exponent, while it has to be used with caution, can be applied to hint toward the predictability of a system [19]. For the time-series friction data in Figs. 1(b)–1(e), the largest Lyapunov exponents are 0.38, 0.16, 0.18, and 1.45, respectively. These positive values indicate a significant degree of chaos within the tribological system [20]. This is not surprising, as even a simple dry friction oscillator model is known to exhibit chaotic behavior [21]. Future research might chart a promising path toward models akin to weather forecasting, where integrating diverse scales and factors enables predictive insight into tribological behavior in technologically relevant systems. A quantitative physical model for the coupled behavior of these factors is not yet available; however, the present findings further highlight that our understanding of real surface topography [22], and of its role in friction and wear, may still be at an early stage. At the same time, the results in this contribution provide a practical basis for future mechanics modeling to clarify how surface topography influences friction and wear.

Our data demonstrate that three physical conditions—a negative oscillation slope, a positive surface profile height Z score, and a positive surface curvature—contribute to the occurrence of high friction. While surface topography [13] and oscillations [23] are not new to tribological studies, elucidating the mechanisms underlying the physical conditions we identified remains a challenge that calls for collective efforts from the community. Nevertheless, it is possible to develop

meaningful heuristics [High Friction Prediction in Figs. 4(a)–4(d) and Fig. S7 of the Supplemental Material [27]] to, for example, predict where the highest friction forces will be present on a given surface profile. By leveraging AI, these predictions can be further refined *[AI High Friction Predictor* in Figs. 4(f)–4(i) and Fig. S8 of the Supplemental Material [27]]. Our findings have been achieved for a wide range of tribological environments, using interfacial media from unadditived base oils to aerospace greases, fully formulated engine oils, and abrasive slurries. While these conditions might seem to amplify the already chaotic nature of tribological systems, it is surprising to find such clear commonalities between them. The AI-based prediction of high-friction regions works surprisingly well despite the generally chaotic nature of tribology. For example and very strikingly, peak friction under grease lubrication [in Fig. 4(i)] can be accurately inferred using data from experiments with three entirely different lubricants.

Even more surprisingly, these physical mechanisms, identified under flat-on-flat contact, remain valid when the contact geometry is changed to a ball-on-flat configuration (Fig. 5). Such a comparison is typically challenging, as these two contact geometries are generally regarded as fundamentally distinct contact configurations.

In processing the surface profile and oscillation data, we deliberately suppressed high-frequency small-scale roughness (e.g., the surface profiles analyzed had a spatial resolution of 1.1 mm). Unlike most traditional models that focus on either individual atomic asperities [24,25] or macroscale statistical averages [17,18], our framework specifically targets mid-scale surface topography. This choice directly responds to calls to recognize the critical role of scale in roughness analysis [22] and represents an important step toward addressing the persistent "mesoscale gap" in friction [26]. By identifying previously overlooked mid-scale features, a positive surface height Z score, positive surface curvature, and a negative oscillation slope, our approach achieves over 80% spatial accuracy in predicting high-friction regions across disparate lubrication scenarios and contact geometries.

V. CONCLUSIONS

Through direct experimental evidence, we demonstrate that the long-standing problem of friction irreproducibility originates from inherently chaotic nature of friction, arising from its extreme sensitivity to minute variations in surface topography and misalignment-induced oscillations. By identifying and coupling three deterministic physical markers, positive surface height Z score, positive surface curvature, and a negative oscillation slope, we establish a predictive framework that achieves over 80% spatial accuracy in locating-high friction regions, and further enhanced its performance with machine learning. The fact that these markers remain effective across disparate lubrication scenarios and different contact geometries indicates a generalized underlying physical mechanism. Academically, our work offers new perspectives on how mid-scale topography is coupled with friction. Practically, high friction and wear can be predicted with over 80% accuracy from surface topography measurements at only 1.1 mm resolution, without the need for elaborate experimental techniques—making this approach readily applicable to a strategic surface design and proactive maintenance strategies in engineering practice.

ACKNOWLEDGMENTS

We express our gratitude to J. Schneider and N. Garabedian for laboratory help and discussions. C.G. would like to acknowledge financial support from the European Research Council (ERC) under Grant No. 771237 and the Deutsche Forschungsgemeinschaft (DFG, German Research Foundation) under Grant No. GR 4174/12, as well as funding through a Future Fields grant from KIT.

DATA AVAILABILITY

The raw data, along with the code used for the evaluation, are published on KITopen [28]. The data that support the findings of this article are openly available [28].

[1] K. Holmberg and A. Erdemir, Influence of tribology on global energy consumption, costs and emissions, Friction **5**, 263 (2017).

[2] R. W. Carpick, A. Jackson, W. G. Sawyer, N. Argibay, P. Lee, A. Pachon, and R. M. Gresham, The tribology opportunities study: Can tribology save a quad? Tribol. Lubr. Technol. **72**, 44 (2016).

[3] M. Watson *et al.*, An analysis of the quality of experimental design and reliability of results in tribology research, Wear **426–427**, 1712 (2019).

[4] C. E. Morstein, A. Klemenz, M. Dienwiebel, and M. Moseler, Humidity-dependent lubrication of highly loaded contacts by graphite and a structural transition to turbostratic carbon, Nat. Commun. **13**, 5958 (2022).

[5] C. Haug, F. Ruebeling, A. Kashiwar, P. Gumbsch, C. Kübel, and C. Greiner, Early deformation mechanisms in the shear affected region underneath a copper sliding contact, Nat. Commun. **11**, 839 (2020).

[6] V. Slesarenko and L. Pastewka, The bumpy road to friction control, Science **383**, 150 (2024).

[7] A. Aymard, E. Delplanque, D. Dalmas, and J. Scheibert, Designing metainterfaces with specified friction laws, Science **383**, 200 (2024).

[8] H. Czichos, S. Becker, and J. Lexow, Multilaboratory tribotesting: Results from the Versailles Advanced Materials and Standards programme on wear test methods, Wear **114**, 109 (1987).

[9] T. D. B. Jacobs, L. Pastewka, and Guest Editors, Surface topography as a material parameter, MRS Bull. **47**, 1205 (2022).

[10] A. R. Hinkle, W. G. Nöhring, R. Leute, T. Junge, and L. Pastewka, The emergence of small-scale self-affine surface roughness from deformation, Sci. Adv. **6**, eaax0847 (2020).

[11] R. Aghababaei, E. E. Brodsky, J.-F. Molinari, and S. Chandrasekar, How roughness emerges on natural and engineered surfaces, MRS Bull. **47**, 1229 (2022).
[12] S. Iida, T. Nagai, and T. Uchiyama, Standard wafer with programed defects to evaluate the pattern inspection tools for 300-mm wafer fabrication for 7-nm node and beyond, J. Micro/Nanolith. MEMS MOEMS **18**, 023505 (2019).
[13] L. Pastewka and M. O. Robbins, Contact between rough surfaces and a criterion for macroscopic adhesion, Proc. Natl. Acad. Sci. USA **111**, 3298 (2014).
[14] H. Yue, J. Schneider, B. Frohnapfel, and P. Gumbsch, The influence of pin inclination on frictional behaviour in pin-on-disc sliding and its implications for test reliability, Tribol. Int. **200**, 110083 (2024).
[15] I. Garcia-Prieto, M. D. Faulkner, and J. R. Alcock, The influence of specimen misalignment on wear in conforming pin on disk tests, Wear **257**, 157 (2004).
[16] M. A. Chowdhury and M. Helali, The effect of amplitude of vibration on the coefficient of friction for different materials, Tribol. Int. **41**, 307 (2008).
[17] M. Marian, M. Bartz, S. Wartzack, and A. Rosenkranz, Non-dimensional groups, film thickness equations and correction factors for elastohydrodynamic lubrication: A review, Lubricants **8**, 95 (2020).
[18] J. A. Greenwood and J. B. P. Williamson, Contact of nominally flat surfaces, Proc. R. Soc. London. A 295, 300 (1966).
[19] M. T. Rosenstein, J. J. Collins, and C. J. De Luca, A practical method for calculating largest Lyapunov exponents from small data sets, Physica D **65**, 117 (1993).
[20] C. Ding, H. Zhu, G. Sun, Y. Zhou, and X. Zuo, Chaotic characteristics and attractor evolution of friction noise during friction process, Friction **6**, 47 (2018).
[21] G. Licskó and G. Csernák, On the chaotic behaviour of a simple dry-friction oscillator, Math. Comput. Simul. **95**, 55 (2014).
[22] A. Pradhan *et al.*, The Surface-topography challenge: A multi-laboratory benchmark study to advance the characterization of topography, Tribol. Lett. **73**, 110 (2025).
[23] T. Dimond, A. Younan, and P. Allaire, A review of tilting pad bearing theory, Int. J. Rotating Mach. **2011**, 1 (2011).
[24] E. Riedo, F. Lévy, and H. Brune, Kinetics of capillary condensation in nanoscopic sliding friction, Phys. Rev. Lett. **88**, 185505 (2002).
[25] A. J. Weymouth, E. Riegel, O. Gretz, and F. J. Giessibl, Strumming a single chemical bond, Phys. Rev. Lett. **124**, 196101 (2020).
[26] A. Vanossi, N. Manini, M. Urbakh, S. Zapperi, and E. Tosatti, *Colloquium*: Modeling friction: From nanoscale to mesoscale, Rev. Mod. Phys. **85**, 529 (2013).
[27] See Supplemental Material at http://link.aps.org/supplemental/10.1103/bx4g-8647 for materials, methods, and evaluation details, which includes Refs. [13,19,29–34].
[28] Y. Li, Raw data and codes to manuscript "Forecasting friction behavior despite its chaotic nature," (2025), https://doi.org/10.35097/75SEAWP9105YJV6J.
[29] M. D. Weir, J. Hass, and G. B. Thomas, *Thomas' Calculus: Early Transcendentals*, (Pearson, Boston, 2014), 13th ed.
[30] *Encyclopedia of Measurement and Statistics*, edited by N. J. Salkind and K. Rasmussen (SAGE Publications, Thousand Oaks, Calif, 2007).
[31] E. N. Lorenz, Deterministic nonperiodic flow, J. Atmos. Sci. **20**, 130 (1963).
[32] F. Takens, Detecting strange attractors in turbulence, in *Dynamical Systems and Turbulence, Warwick 1980*, edited by D. Rand and L.-S. Young (Springer, Berlin, 1981), Vol. 898, pp. 366–381.
[33] Z. Zhang, Introduction to machine learning: *K*-nearest neighbors, Ann. Transl. Med. **4**, 218 (2016).
[34] Y. Li, N. Garabedian, J. Schneider, and C. Greiner, Waviness affects friction and abrasive wear, Tribol. Lett. **71**, 64 (2023).